actuators

MDPI

Article

Analysis and Structure Optimization of Scissor-Type Micro-Stirrer with the Most Effective Output Performance for Thrombus Dissolution in Interventional Therapy

Jingjing Yang [1], Benyang Rong [1], Lei Wang [1], Minoru Morita [2], Guifang Deng [1], Yifan Jiang [1] and Junbing Qian [1,*]

[1] Faculty of Civil Aviation and Aeronautics, Kunming University of Science and Technology, Kunming 650500, China
[2] Graduate School of Science and Engineering, Yamaguchi University, Yamaguchi 7558611, Japan
* Correspondence: 20140013@kust.edu.cn; Tel.: +86-871-65919402

Abstract: Compared with thrombus dissolution using only thrombolytic agents, an advanced therapy of direct stirring of the blood clot can yield shorter recanalization time and higher recanalization velocity. Our previous research presented the design of a novel micro-stirrer, which can convert longitudinal vibration into transverse vibration and eventually generate opposite transverse vibration at the end-effort, like a scissor, for efficient blood clot stirring and thrombus dissolution acceleration. Transverse vibration is the most effective movement to dissolve thrombi. However, the small size of blood vessels has strict limits, which will greatly affect the output transverse vibration. Therefore, to improve the output performance of the micro-stirrer in curved and narrow vascular spaces, the analysis and structure optimization of the micro-stirrer is expected to increase the vibration mode conversion efficiency from longitudinal to transverse mode. The design concept and theoretical analysis of the micro-stirrer are presented in detail. Aiming to obtain the optimal structure parameters of the micro-stirrer, the mathematical model is established and analyzed. Next, a series of finite element models involving important structure parameters are designed and investigated. Finally, the optimal structure parameters are obtained, and the stirring effect in a blood vessel is verified by simulation and experiment.

Keywords: structure optimization; micro-stirrer; mode conversion; output performance; thrombus dissolution

check for updates

Citation: Yang, J.; Rong, B.; Wang, L.; Morita, M.; Deng, G.; Jiang, Y.; Qian, J. Analysis and Structure Optimization of Scissor-Type Micro-Stirrer with the Most Effective Output Performance for Thrombus Dissolution in Interventional Therapy. *Actuators* **2023**, *12*, 60. https://doi.org/10.3390/act12020060

Academic Editor: Katsushi Furutani

Received: 27 December 2022
Revised: 23 January 2023
Accepted: 25 January 2023
Published: 30 January 2023

Copyright: © 2023 by the authors. Licensee MDPI, Basel, Switzerland. This article is an open access article distributed under the terms and conditions of the Creative Commons Attribution (CC BY) license (https://creativecommons.org/licenses/by/4.0/).

1. Introduction

The continuous improvement of living conditions and unhealthy lifestyles has led to the rise of cerebral stroke as one of the leading mortality causes worldwide [1,2]. Failure of timely removal of the thrombus will cause tissue damage resulting in language impairment, physical disabilities and death [3,4]. The most common therapeutic method is thrombolytic agent injection. However, a high dose of a thrombolytic agent may lead to hemorrhage, whereas a small dose means a longer recanalization time [5–7]. Moreover, the strict time window of thrombolytic therapy within three to six hours after the stroke symptoms restricts the thrombolysis opportunity for most patients [8–11].

To overcome the inability to receive thrombolytic therapy, many types of mechanical thrombectomy devices, such as Merci Retriever and Solitaire Flow Restoration, have been designed and applied for rapid vascular recanalization [12–16]. These devices have the advantages of a longer time window, higher rate of recanalization and clinical outcomes than thrombolysis. However, the intima damage to blood vessels was found when the unfolded stent threaded through the blood vessel [17]. Moreover, the current devices are more suitable to be used in relatively larger blood vessels with a diameter bigger than 2 mm [18]. A new advanced approach among the mechanical thrombectomy devices is to design a micro-stirrer that can produce effective transverse vibration in narrow and

curved blood vessels to crush and stir the thrombus with the injection of a low-dose thrombolytic agent around the thrombus [19,20]. Since the mechanical vibration directly destroys the surface structure of the blood clot and increases the contact area between the agent and clot, higher recanalization velocity and shorter therapy time are achieved. However, some blood vessels are tiny (<2 mm), which severely limits the applied power, structure and size of the micro-stirrer. Considering the small diameter and curved shape of blood vessels, designing a micro-stirrer with enough power and vibration displacement is a challenge. In our previous research, a scissor-type micro-stirrer comprising a powerful transducer and a slender wire-type micro-stirrer with a special end-effort was successfully designed [21,22]. A transducer that can excite longitudinal elastic waves as the driving force was selected because longitudinal waves can travel longer distances with less attenuation than shear elastic waves [23]. The transducer was placed extracorporeally with no size restriction, so it is able to supply a driven force that is as large as possible. The driven energy excited by the transducer can be transmitted far and reach the end-effort, then vibration mode conversion from longitudinal vibration to transverse vibration occurs due to the special structure design of the end-effort based on Snell's law. Finally, the effective stir function is concentrated at the stirrer tip only (Figure 1). Considering the size and shape of blood vessels have strict limits, the excitation of effective output transverse vibration is difficult. However, the transverse vibration is the most effective motion to dissolve thrombi. Therefore, the detailed analysis and structure optimization of the micro-stirrer for increasing the conversion efficiency from longitudinal mode to the transverse mode in curved and narrow blood vessels are urgently required.

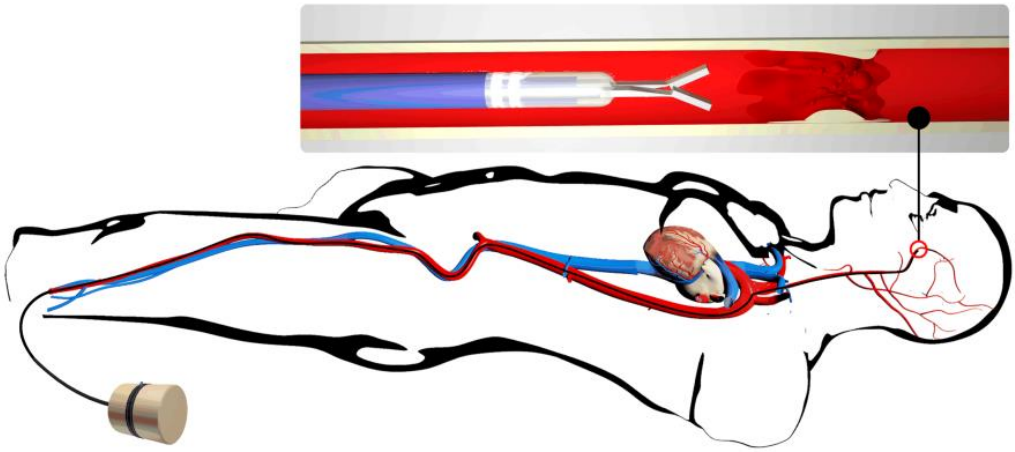


Figure 1. Working schematic of scissor-type micro-stirrer in interventional therapy.

This paper presents the structural optimization method for the scissor-type micro-stirrer, which can maximize output performance with the highest transverse vibration displacement. The design concept is presented, and the mathematical modeling of the micro-stirrer is developed and analyzed. Several finite element models involving important structure parameters are established to investigate the highest conversion efficiency from longitudinal vibration mode to transverse vibration mode. Finally, the optimal design parameters of the micro-stirrer are obtained, and the stirring performance is assessed by both simulations and experiments.

2. Design Concept and Evaluation

2.1. Concept of Structure Design

In thrombus dissolution therapy, the initial design of the micro-stirrer included a shear-actuated cantilever beam and a piezoelectric plate which can generate transverse vibration at the beam tip for accelerating clot dissolution with the injection of a low-dose thrombolytic agent [20]. The transverse vibration of the micro-stirrer tip enables stirring and crushing functions for stirring the blood clot and fully mixing clots with the agent,

which accelerates dissolution with a low risk of hemorrhagic complications in a short time. Because the tip deflection of a cantilever beam is proportional to its length, the cantilever beam should be long enough to generate transverse vibration as high as possible. However, owing to the small size of blood vessels, obtaining adequate tip transverse vibration with a short cantilever beam is challenging. Moreover, because blood vessels have a lot of curves, the unnecessary transversal deflection of the cantilever beam, except for the tip deflection, will lead to loss of energy and damage at the intima of the blood vessel.

A wire-type micro-stirrer is hereby proposed, which can transmit longitudinal elastic waves from an external transducer to the stirrer tip and convert the longitudinal vibration into transverse vibration just at the end-effort [23]. The longitudinal elastic wave excited by the transducer is transmitted through the long distance of the beam and reaches the groove. Then, part of the longitudinal elastic wave impinges on the slant surface of the groove and changes direction based on Snell's law, which induces transverse vibration at the end-effort only (Figure 2). In this design, the transducer is placed outside of the body without size restriction so that enough driven force can be supplied. However, in this design, the desired vibration mode can be achieved only for a given proportion of end-effort length and the entire stirrer length (Equation (1)) [24]. Therefore, this design cannot provide a stable vibration mode, and the micro-stirrer size cannot be adjusted discretionarily for applications in different blood vessels.

$$\zeta = \frac{L_E^2}{L_S} = \frac{\gamma_e^2 h}{(2n-1)\pi\sqrt{3}}, \tag{1}$$

where ζ is the length ratio for the desired vibration mode, L_E is the length of the end-effort, L_S is the entire length of the micro-stirrer, n is the mode shape number, γ_e is the root of the frequency characteristic equation of the cantilever beam at the second mode with value of 4.694 and h is the beam thickness.

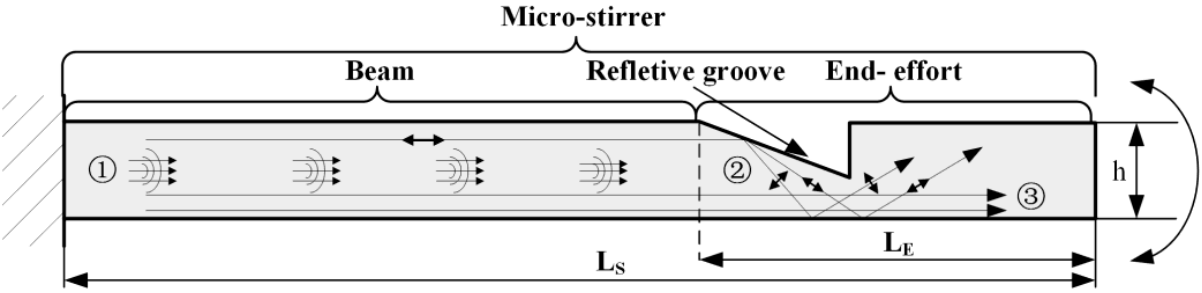


Figure 2. Schematic diagram of micro-stirrer ① Input longitudinal elastic wave, ② Mode conversion from longitudinal to transversal vibration, ③ Propagating longitudinal elastic wave.

To address the above problem, a new design is hereby proposed (Figure 3). In this case, the end-effort is separated into two slight beams by creating a crack along the center line, and two reflective grooves are cut on the opposite surfaces of the slight beams. As the longitudinal elastic wave reaches the grooves, part of it will be reflected and converted into a shear wave, which will produce out-of-phase bending moments at the end-effort and make it work like a scissor. Simultaneously, these two moments will bend the beam in opposite directions and counteract each other. Therefore, the bending part will concentrate on the end-effort only without unnecessary deflection on other parts.

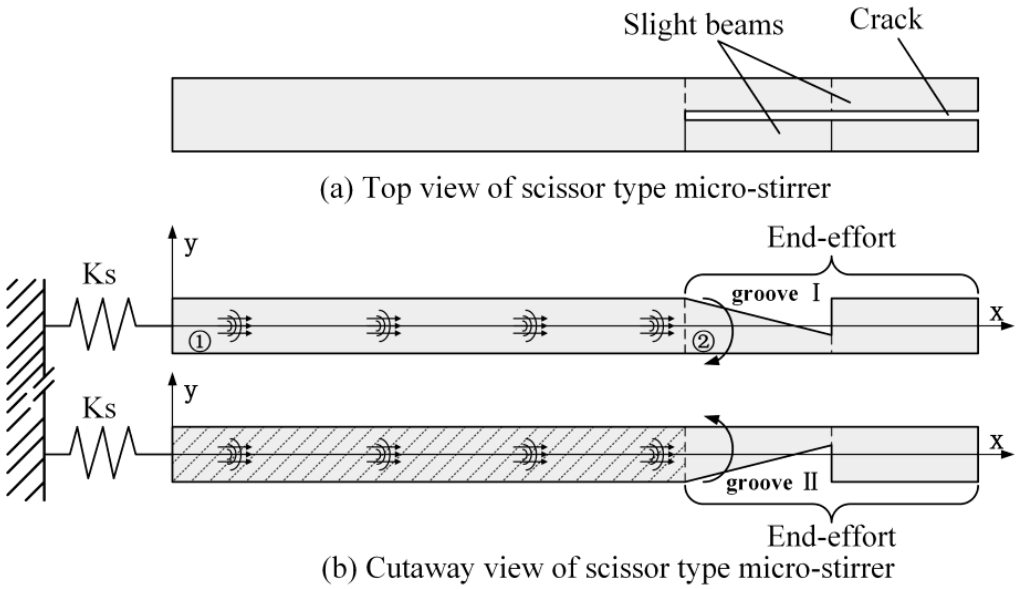


Figure 3. Theoretical model of scissor-type micro-stirrer ① Longitudinal driven force, ② Bending moment at the reflective groove.

2.2. Evaluation of Stirrer Design

The effectiveness of the design was assessed using a finite element model of the scissor-type micro-stirrer built by Comsol Multiphysics software (Figure 4). In order to reduce computation time, the total length of the micro-stirrer was shortened. The length, width and thickness of the micro-stirrer were 90 mm, 2 mm and 1 mm, respectively. A piezoelectric stack (PZT) with a length of 10 mm was connected at the left end of the micro-stirrer, polarized along the length direction. The material of the micro-stirrer in the model is titanium which is the common material used for guide wire in interventional therapy. In the simulation, the PZT, which comprises several ceramic slices of lead zirconate titanate, was simplified as an integrated structure, and the groove angle was set as 80° at first. The left end of the PZT is fixed, whereas the other boundaries are free. The details of each parameter are listed in Table 1.

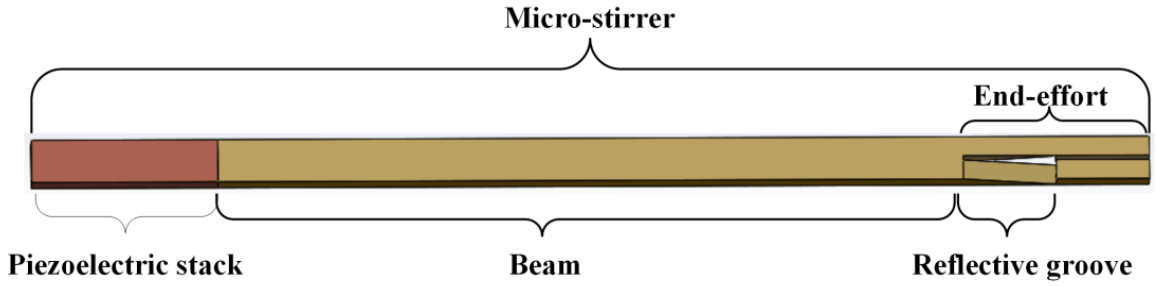


Figure 4. Schematic diagram of the scissor-type micro-stirrer.

To assess the proposed design, Eigen frequency analysis, harmonic analysis and transient analysis were conducted, respectively. Figure 5 shows that there is a considerable scissor-type deflection at the resonance frequency of 2015.4 Hz, in which the bending part concentrates on the beam tip while generating negligible deflection on the other part. In contrast with the scissor-type mode, the other two mode shapes excited at resonance frequencies of 1319.6 Hz and 2282 Hz both produced obvious deflection on the entire stirrer. These two frequencies will produce unnecessary transverse vibration in the blood vessels.

Table 1. Parameters of FEM model.

Parameters	Value	Unit
Material	Titanium	—
Young's modulus (E)	115.7	GPa
Density (ρ)	4540	Kg/m^3
Poisson's ratio (ν)	0.32	—
Length of stirrer	90	mm
Length of end-effort	10	mm
Length of groove	5	mm
Length of PZT	10	mm
Width	2	mm
Thickness	1	mm
Groove angle	80	degree

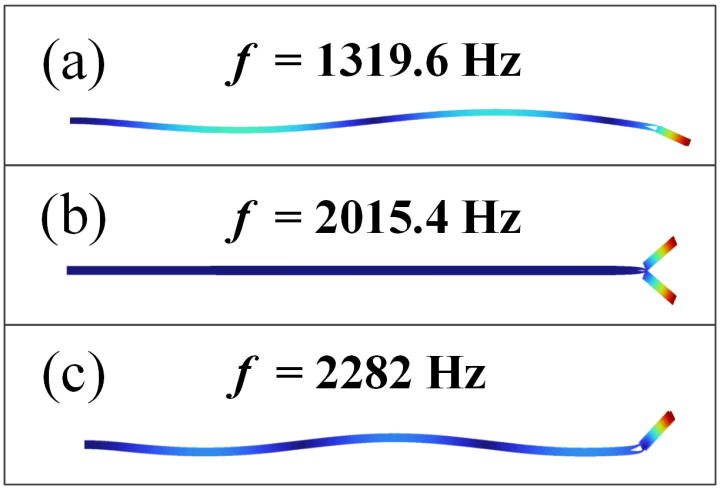


Figure 5. Vibration mode shapes at different response frequencies: (a) f = 1319.6 Hz (b) f = 2015.4 Hz (c) f = 2282 Hz.

Harmonic analysis was performed to analyze the vibrational state in detail. Figure 6 shows the transversal displacements of the stirrer tip and beam driven by sweep frequency ranging from 1300 Hz to 2450 Hz with a voltage of 20 V added at the PZT. A maximum vertical deflection with a value of 1.44×10^{-4} mm is excited at the tip (point A) under the response frequency of 2015.4 Hz, and the deflection on the beam (point B) is negligible. In contrast with the scissor-type mode, the other two vibration modes excite small vertical deflections at all resonant frequencies, further demonstrating the design effectiveness of the scissor-type micro-stirrer.

Furthermore, a transient analysis was performed by adding a sinusoidal voltage of 20 V at the resonant frequency of 2015.4 Hz. The actual vibration of the micro-stirrer, as well as the deflection stability of the model, were thus evaluated. The transversal displacement of the two tips (point A_1 and A_2) and one beam point (point B) are simulated from 0–40 ms with 0.01 ms intervals. As shown in Figure 7, the curves begin with a small deflection which indicates the delay time of the oscillation start. A larger deflection is excited successfully with time, with a maximal amplitude of 1.44×10^{-4} mm, which coincides with the results of the harmonic analysis. The phase positions of these two tips (point A_1 and A_2) are opposite, which confirms the stability of the scissor-type vibration mode. Meanwhile, the transversal displacement of the beam is almost zero, which further confirms that longitudinal vibrations are effectively converted into tip deflection concentrated at the end-effort.

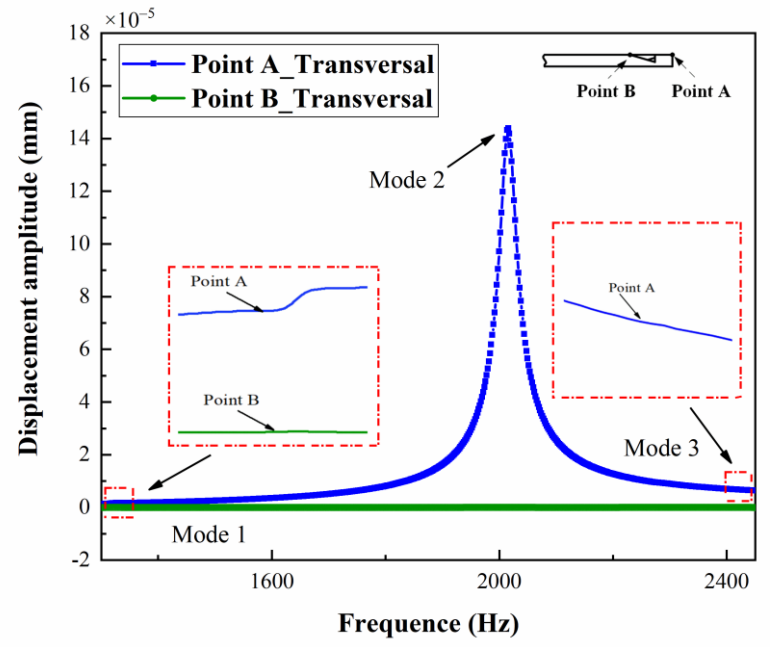


Figure 6. The transversal amplitudes of the microstirrer at the stirrer tip and beam.

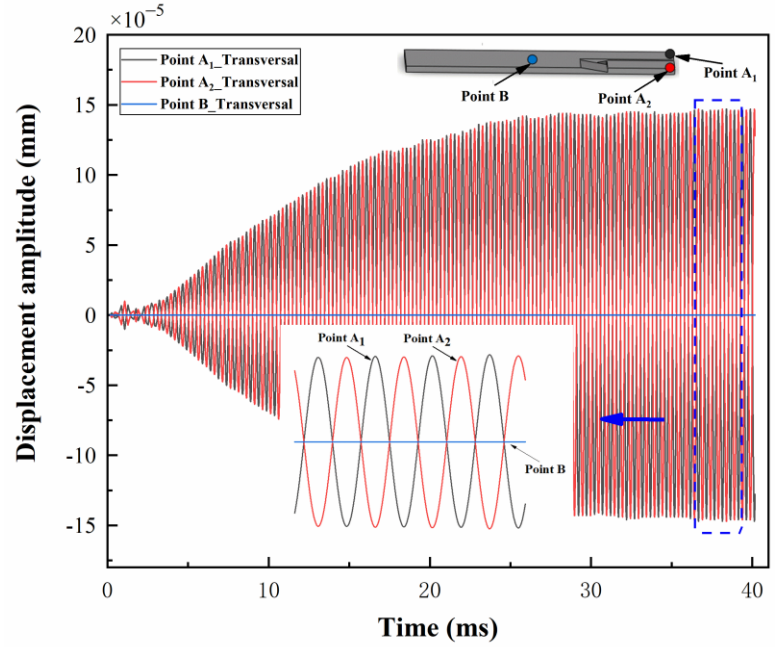


Figure 7. The transversal vibration displacements of the micro-stirrer at different points vs. time.

Considering the vascular environment is complex and diverse, various end-effort lengths should be available to adapt to different sizes of blood vessels. In addition, due to the different environments in which thrombi are formed, mechanical properties of blood clots, such as hardness, show notable variation. Therefore, the micro-stirrer should be able to apply different forces, amplitudes and resonance frequencies according to surgery demands. The driven force could be adjusted by the input voltage of the external transducer, which is feasible in this design. Under the same boundary condition, three models with arbitrary lengths of the end-effort, namely 8 mm, 10 mm and 14 mm, are simulated. The other parameters are the same as listed in Table 1. Figure 8 shows that the scissor-type modes are excited successfully in all models with resonant frequencies of 3790 Hz, 2015.4 Hz and 904.1 Hz, respectively. The simulation results indicate that the desired scissor-type mode can be successfully obtained with arbitrary sizes, which demonstrates

the reliability and stability of the proposed design. Moreover, the output frequency and length of the end-effort can be easily adjusted by changing the structure parameters for different surgery demands.

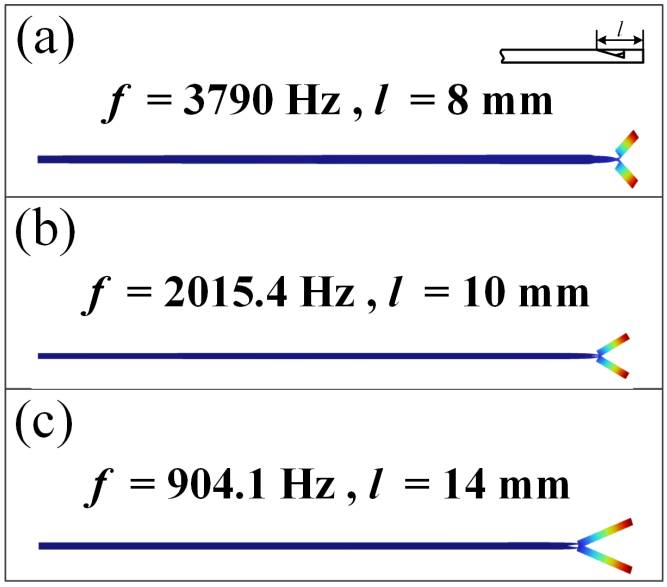


Figure 8. Mode shape simulations with arbitrary lengths of end-efforts: (a) l = 8 mm (b) l = 10 mm (c) l = 14 mm.

3. Structure Modeling and Optimization

3.1. Mathematical Modeling

A simplified dynamic model is established to investigate the characteristics of the designed micro-stirrer. Considering that the proposed micro-stirrer has two vibration modes at the beam and end-effort, respectively, the dynamic model is simplified and divided into the longitudinal part and the transversal part (Figure 9). Each part of the designed micro-stirrer can be modeled as a mass-spring system. The longitudinal part of the dynamic model is a beam with a spring (k_s) at the left end and a mass (m_c) connected at the right end. For transversal vibration mode, since the bending deflection concentrates on the reflective grooves, the groove is replaced by a simple beam, and the left end of the groove connects with a torsional spring (k_t) to simulate the bending movement. Additionally, the tip of the end-effort is replaced by another mass (m_a/m_b).

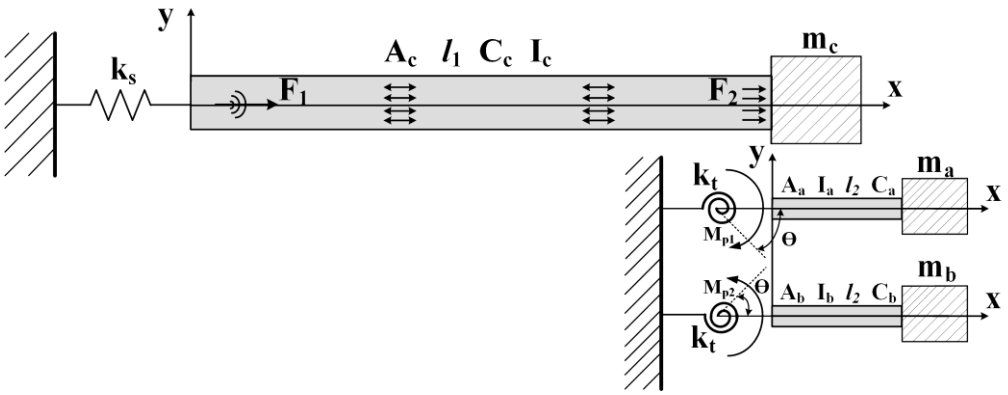


Figure 9. Simplified dynamic model of scissor-type micro-stirrer.

The motion equations of the longitudinal and transversal vibration modes can be expressed as

$$[\rho A_c + m_c\delta(x-l_1)]\frac{\partial^2 u}{\partial t^2} - EA_c\left[\frac{\partial^2 u}{\partial x^2} + C_c\frac{\partial^3 u}{\partial x_1^2\cdot\partial t}\right] = F_1\delta(x-0) - k_s u\delta(x-0), \quad (2)$$

$$[\rho A_a + m_a\delta(x-l)]\frac{\partial^2 y}{\partial t^2} + \frac{\partial^2}{\partial x^2}[EI_a(1+C_a\frac{\partial}{\partial t})\frac{\partial^2 y}{\partial x^2}] = M_{p1}\delta'(x-l_1) - k_t\theta\delta'(x-l_1), \quad (3)$$

$$[\rho A_b + m_b\delta(x-l)]\frac{\partial^2 y}{\partial t^2} + \frac{\partial^2}{\partial x^2}[EI_b(1+C_b\frac{\partial}{\partial t})\frac{\partial^2 y}{\partial x^2}] = M_{p2}\delta'(x-l_1) - k_t\theta\delta'(x-l_1), \quad (4)$$

where A_a, A_b and A_c are the cross-section areas of the groove and beam, respectively, ρ is the mass density, E is Young's elastic modulus, u is the longitudinal vibrational displacement of the beam, y is the transversal vibrational displacement of the end-effort, δ is the Dirac coefficient, F_1 is the input driven force at $x = 0$, M_p is the input torque at the torsional spring, θ is the rotational angle of the torsional spring, I_a, I_b and I_c are the inertia moment of the groove and beam, respectively, $l = l_1 + l_2$, where l_1 is the length of the beam and l_2 is the length of groove and C_a, C_b and C_c are the damping coefficients.

Based on the expansion theorem, a separation-of-variables solution of Equations (2)–(4) yields

$$u(x,t) = \sum_{i=1}^{n} U_i(x)q_i(t), \quad (5)$$

$$y(x,t) = \sum_{i=1}^{n} X_i(x)\cdot f_i(t), \quad (6)$$

Assume that

$$M_{p1} = -M_{p2} = \gamma_1 F_2, \quad (7)$$

$$\theta = \gamma_2 F_2, \quad (8)$$

$$F_2 = EA_c\frac{\partial u}{\partial x} = EA_c\sum_{i=1}^{n}\dot{U}_i(l_1)q_i(t), \quad (9)$$

where γ_1 and γ_2 are force conversion factors. Substituting Equations (5)–(9) into Equations (2)–(4) and applying the Galerkin method to the resulting equations, the motion equations for the complete model can be expressed as

$$\begin{cases} M_c\ddot{q} + T_c\dot{q} + K_c q = P_c F_1 \\ M_a\ddot{F}_a + T_a\dot{F}_a + K_a F_a = P_a q \\ M_b\ddot{F}_b + T_b\dot{F}_b + K_b F_b = P_b q \end{cases}, \quad (10)$$

Equation (10) can be modified in the form of a continuous time state equation as

$$\dot{x}(t) = \begin{bmatrix} -\frac{T}{M} & -\frac{K}{M} \\ I & 0 \end{bmatrix}\cdot x(t) + \begin{bmatrix} \frac{P}{M} \\ 0 \end{bmatrix}\cdot F_1, \quad (11)$$

where

$q = [q_1(t)\ q_2(t)\cdots q_n(t)]^T$, $F_a = [f_{a1}(t)\ f_{a2}(t)\cdots f_{an}(t)]^T$, $F_b = [f_{b1}(t)\ f_{b2}(t)\cdots f_{bn}(t)]^T$

$$
\begin{cases}
m_{cij} = \int_0^{l_1} [\rho A_c + m_c \delta(x - l_1)] U_i(x) U_j(x) dx \\
t_{cij} = \int_0^{l_1} -EA_c C_c \ddot{U}_i(x) U_j(x) dx \\
k_{cij} = \int_0^{l_1} -EA_c \ddot{U}_i(x) U_j(x) dx + \int_0^{l_1} k_s U_i(x) U_j(x) \delta(x - 0) dx \\
P_{cij} = \int_0^{l_1} U_j(x) \delta(x - 0) dx
\end{cases}
$$

$$
\begin{cases}
m_{a/b\ ij} = \int_{l_1}^{l} [\rho A_{a/b} + m_{a/b} \delta(x - l)] \cdot X_i(x) X_j(x) dx \\
t_{a/b\ ij} = \int_u^{l} EI_{a/b} C_{a/b} \ddot{\ddot{X}}_i(x) X_j(x) dx \\
k_{a/b\ ij} = \int_{l_1}^{l} EI_{a/b} \ddot{\ddot{X}}_i(x) X_j(x) dx \\
P_{aij} = \int_{l_1}^{l} (\gamma_1 - k_t \gamma_2) \cdot EA_c \cdot \dot{U}_i(l_1) \cdot U_j(x) \cdot \dot{\delta}(x - l_1) dx \\
P_{bij} = \int_{l_1}^{l} (-\gamma_1 - k_t \gamma_2) \cdot EA_c \cdot \dot{U}_i(l_1) \cdot U_j(x) \cdot \dot{\delta}(x - l_1) dx
\end{cases}
$$

$$
M = \begin{bmatrix} M_c & 0 & 0 \\ 0 & M_a & 0 \\ 0 & 0 & M_b \end{bmatrix}
$$

$$
T = \begin{bmatrix} T_c & 0 & 0 \\ 0 & T_a & 0 \\ 0 & 0 & T_b \end{bmatrix}
$$

$$
K = \begin{bmatrix} K_c & 0 & 0 \\ -P_a & K_a & 0 \\ -P_b & 0 & K_b \end{bmatrix}
$$

$$
P = \begin{bmatrix} P_c \\ 0 \\ 0 \end{bmatrix}
$$

The motion equations show that the output displacement mainly depends on the input force F_1, force conversion factor γ, stiffness matrix K and mass matrix M. Furthermore, input force F_1 can be adjusted by input voltage, so the analysis in this paper will not focus on it. Whereas the force conversion factor mainly depends on the groove structure, especially the angle of the reflective groove. Therefore, the structural parameter optimization of the micro-stirrer should focus on the analysis of the reflection angle, inertia mass and stiffness.

3.2. Structure Parameters Optimization

Because the activity environment of the micro-stirrer is blood vessels, the size of the stirrer has strict limits, which will greatly affect the performance of mode conversion. Therefore, the optimal structural parameters should be obtained. Based on the above dynamic model, the structure parameters involving the angle of reflective groove, inertia mass and stiffness have a notable impact on output performance. To obtain the structure with the highest output transversal vibration, several simulation models are designed and analyzed to achieve optimal structural parameters.

3.2.1. Incident Angle

The angle of the reflective groove equals the incident angle of the longitudinal elastic wave, based on the structure of the scissor-type micro-stirrer. According to Snell's law, the mode conversion from longitudinal to shear wave occurs when the longitudinal wave impinges an interface of two different media [25]. As illustrated in Figure 10, the longitudinal elastic wave (Li) excited by the transducer impinges the titanium-air interface and reflects as a longitudinal wave (Lr) and shear wave (Sr) in an approximately vertical direction. This phenomenon can be effectively utilized to convert longitudinal vibration to transversal vibration at the stirrer tip, enabling vibration mode conversion. The equations governing Snell's law and mode conversion with respect to the longitudinal wave incident angle θ are

given in Equations (12)–(14) [25]. Based on these equations, the reflection coefficients of the longitudinal wave and shear waves can be calculated, as shown in Figure 11.

$$\frac{V_L}{\sin\theta} = \frac{V_s}{\sin\varphi}, \tag{12}$$

$$R_{ll} = \left[\frac{\cos^2\varphi - (V_S/V_L)^2 \sin 2\theta \ \ \sin 2\varphi}{\cos^2\varphi + (V_S/V_L)^2 \sin 2\theta \ \ \sin 2\varphi}\right]^2, \tag{13}$$

$$R_{sl} = \frac{4(V_S/V_L)^2 \sin 2\theta \ \ \sin 2\varphi \ \ \cos^2 2\varphi}{\left[\cos^2\varphi - (V_S/V_L)^2 \sin 2\theta \ \ \sin 2\varphi\right]^2}, \tag{14}$$

where V_L and V_S are the velocities of the longitudinal and shear waves in the solid, respectively, while R_{ll} and R_{sl} are energy reflection coefficients of the longitudinal and shear waves, respectively. The longitudinal wave velocity and shear wave velocity in titanium are 5090 m/s and 3125 m/s, respectively.

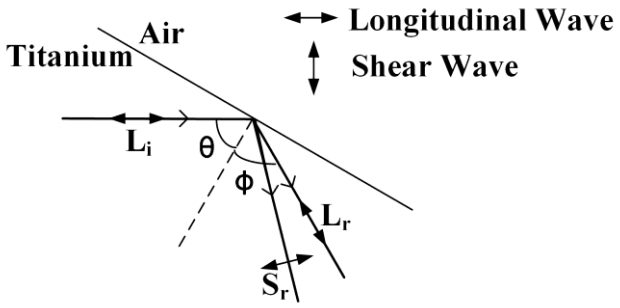


Figure 10. Reflection and mode conversion by an incident longitudinal wave as it impinges a Titanium-Air interface.

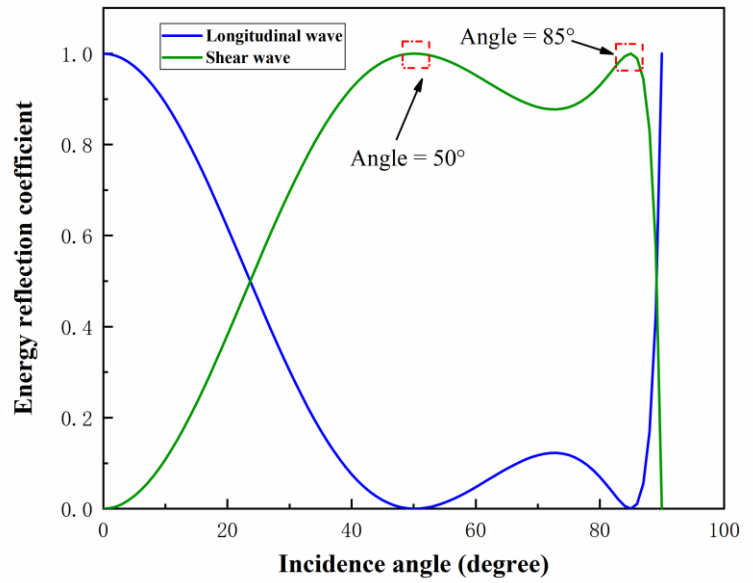


Figure 11. Energy reflection coefficient vs. incidence angle.

Figure 11 shows that the highest energy reflection coefficient of the shear wave is obtained when the incident angles are 50° and 85°, which is the key to achieving high performance. For incident angles less than 50°, the reflection energy cannot reach the stirrer tip. In addition, in this design, some part of the energy will pass through the groove and impact with the reflective shear wave, which will lead to a complicated interference phenomenon. Considering these situations, several models with different incident angles

are tested, with the other structure parameters kept the same as the above model. The transverse amplitudes with different incident angles are shown in Figure 12. The scissor-type structure design produces the highest amplitude at an incident angle of 83°, whereas the amplitude at an incident angle of 85° is much less. Therefore, in this design, the optimal incident angle is determined as 83°.

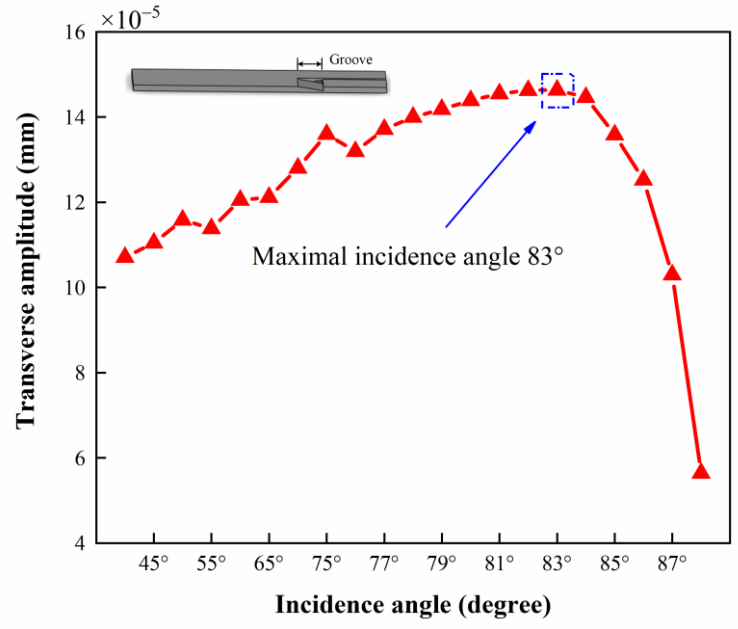


Figure 12. Transverse amplitudes with different incidence angles.

3.2.2. Inertia Mass

Inertia mass is another core parameter that has a crucial influence on output performance. In the above dynamic model and simulation, the deflection concentrates on the reflective groove. The end-effort, except the groove, is simulated as inertia mass to strengthen the vibration. To evaluate the transverse amplitude with different inertia masses, eight models with tip lengths ranging from 1–8 mm are tested. The incident angle is set as the optimal value of 83°. The other parameters are the same, as listed in Table 1.

The simulated results in Figure 13 show that the highest amplitude is excited at the tip length of 6 mm. According to the simulation curve, the amplitude increases as the mass length is less than 6 mm and decreases as the mass length is bigger than 6 mm. In the above simulations, the groove length remained the same along with the mass length, which also affects the conversion efficiency. This means that the inertia mass has a great influence on the mode conversion. However, the optimal inertia mass is not a certain value, which may be changed along with the groove length.

3.2.3. Stiffness

Stiffness is an important parameter to be considered for improving a vibrational structure. The length of the end-effort and groove depth has a direct bearing on structure stiffness, which in turn influences excited amplitude and resonance frequency. The influence of stiffness on the stirrer performance was evaluated by six models with different end-effort lengths and groove depths. The models are divided into two sets with end-effort lengths of 10 mm and 14 mm, with groove depths of 0.6 mm, 0.7 mm and 0.8 mm for each length, respectively. The simulation results are shown in Figure 14. For lengths of end-effort of 10 mm and 14 mm, the highest transversal amplitude occurs when the groove depths are 0.6 mm and 0.7 mm, respectively. It is observed that with the same end-effort length of 10 mm, the transverse amplitude decreases with the increase of groove depth. However, when the length of the end-effort is 14 mm, the max amplitude is excited at the groove depth of 0.7 mm. Moreover, as the end-effort length increases from 10 mm to 14 mm,

the amplitude at 14 mm is not always higher than 10 mm, even if the stiffness decreases, such as for a groove depth of 0.6 mm. Therefore, the output amplitude does not change linearly with the groove depth. In other words, each stirrer with a different end-effort length should be individually analyzed to obtain the optimal groove depth for achieving the best output performance.

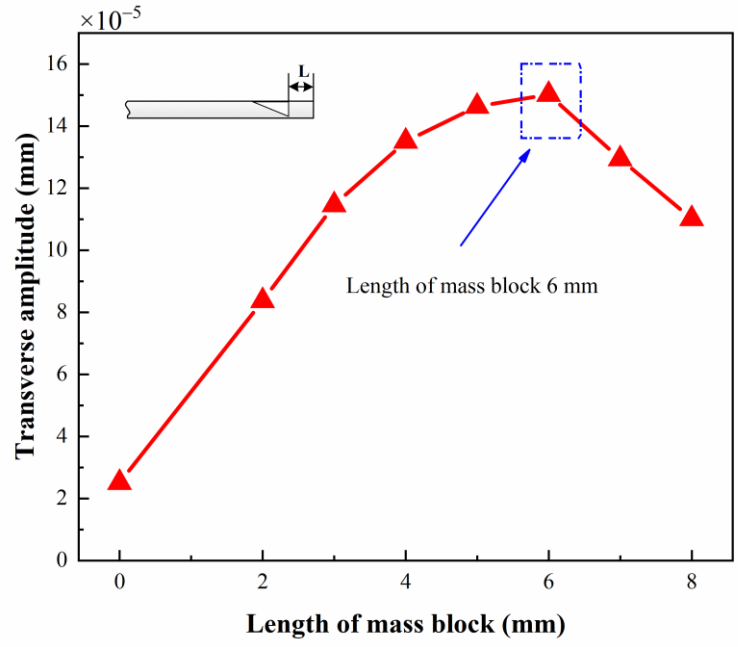


Figure 13. Transverse amplitudes with different inertia masses.

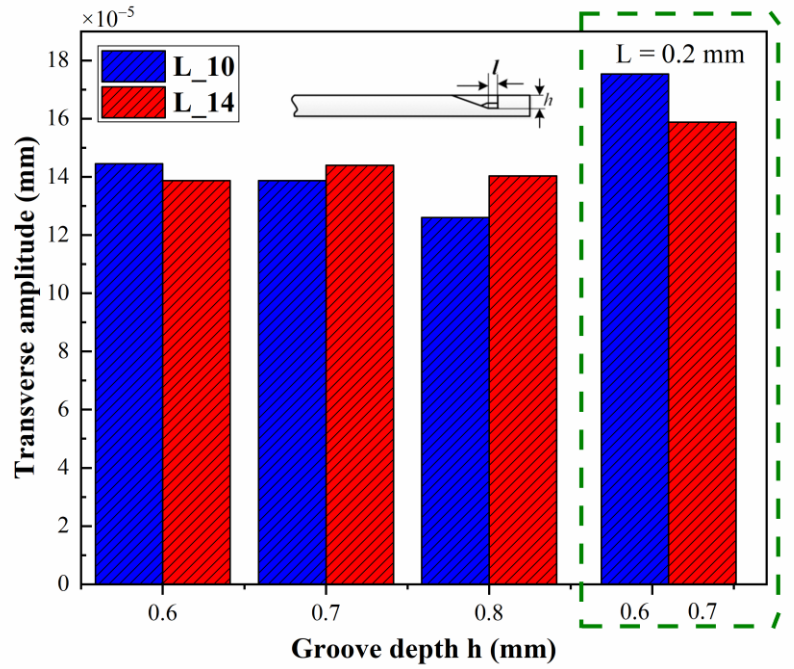


Figure 14. Transverse amplitudes with different lengths of end-effort, groove depth and extended groove length.

The two models with the highest amplitudes are selected and modified to further reduce stiffness and increase the amplitude. Models with groove lengths extended by 0.2 mm are tested. The simulation results showed that both models have higher amplitudes with values of 1.75×10^{-4} mm (L = 10 mm) and 1.59×10^{-4} mm (L = 14 mm). This indicates

that the extended groove length greatly lowers the stiffness to increase the transversal amplitude, which is a good way to improve output performance. All the above simulated results demonstrate that the mode conversion efficiency is not determined by one parameter only, and the optimal structure parameters depend on specific situations.

3.2.4. Inner Hole

The main structural parameters of the scissor-type stirrer for obtaining high output performance were determined in the previous paragraphs. However, in clinical surgery, after crushing and stirring the thrombus, the undissolved fragments should be aspirated out of the body as soon as possible. Since the surgery time affects the effect of recanalization, a micro-stirrer with an inner hole at the beam with both crushing and aspirating functions can effectively shorten the surgery time. On the one hand, an inner hole drilled at the beam may decrease the energy transmission of the longitudinal elastic wave due to the material removal along the transfer path. On the other hand, the inner hole will also decrease the stiffness, which was shown to increase the vibration amplitude. Aiming to evaluate the influence of an inner hole on mode conversion, an inner hole as aspirating tunnel with different radii of 0.2 mm, 0.3 mm and 0.4 mm is cut along the center line of the stirrer beam and simulated. The above optimal structure parameters for reflective angle, end-effort length, groove depth and groove extended length are introduced in the model as 83°, 10 mm, 0.6 mm and 0.2 mm, respectively. The input is a sinusoidal voltage of 20 V under the corresponding resonance frequencies.

Figure 15 shows that the micro-stirrer without an inner hole has the highest mode conversion efficiency with a transversal amplitude of 1.75×10^{-4} mm. However, the relationship between the radius of the inner hole and the transverse amplitude does not decrease linearly. For a radius of 0.3 mm, the mode conversion efficiency decreases to the lowest level with a transversal amplitude of 1.48×10^{-4} mm and then starts to rise to 1.54×10^{-4} mm for a radius of 0.4 mm. Considering the overall structural dimension of the stirrer, the optimal radius with the highest transverse amplitude is a radius of 0.2 mm.

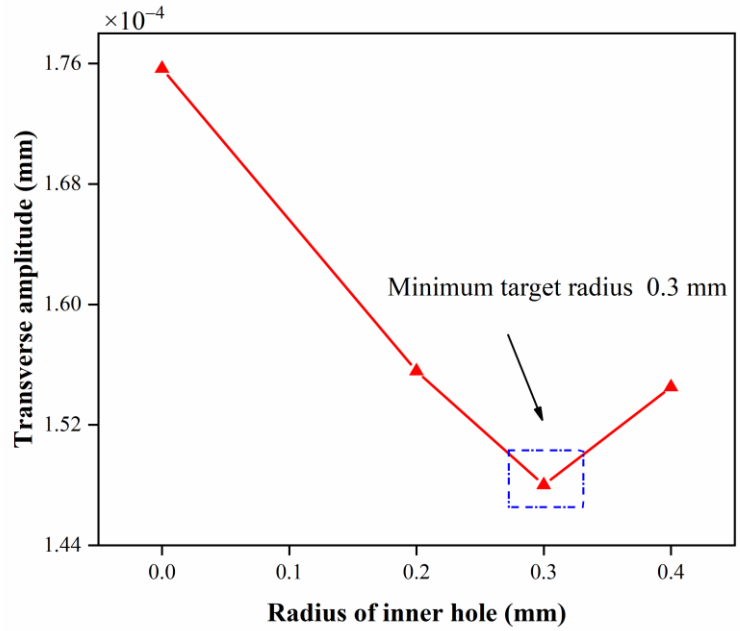


Figure 15. Transverse amplitudes with different radii of inner holes.

Additional evaluation of the final mode conversion efficiency with the optimal inner hole size is conducted through a transient analysis to calculate the motion trajectory of the stirrer tip. To this end, a sinusoidal voltage with an amplitude of 20 V and resonance frequency of 1750.7 Hz is added at the PZT. The stationary vibration data of the motion trajectory of both tips are recorded and plotted from 9 ms to 40 ms. Figure 16 shows that

the motion trajectory of each tip is symmetrical to the *x*-axis, like a scissor, which coincides with the proposed design. The transverse vibration converted at the end-effort is the key to generating effective stirring and mixing of the blood clot with a thrombolytic agent. Simultaneously, as Figure 2 shows, some part of the longitudinal elastic wave passes through the groove and excites longitudinal vibration to crush the thrombus. The longitudinal and transverse amplitudes are 3.53×10^{-5} mm and 1.56×10^{-4} mm, respectively. The transverse amplitude decreased compared with the model without an inner hole, which proves that the material removal reduces the longitudinal force. Figure 16 also shows that as time passes, the vibration trajectory becomes an elliptical vibration which has both knocking and stirring functions to accelerate thrombus dissolution. Therefore, the proposed micro-stirrer can generate stable and reliable scissor-type vibration, as well as higher efficiency than single vibration for cerebral vascular interventional therapy.

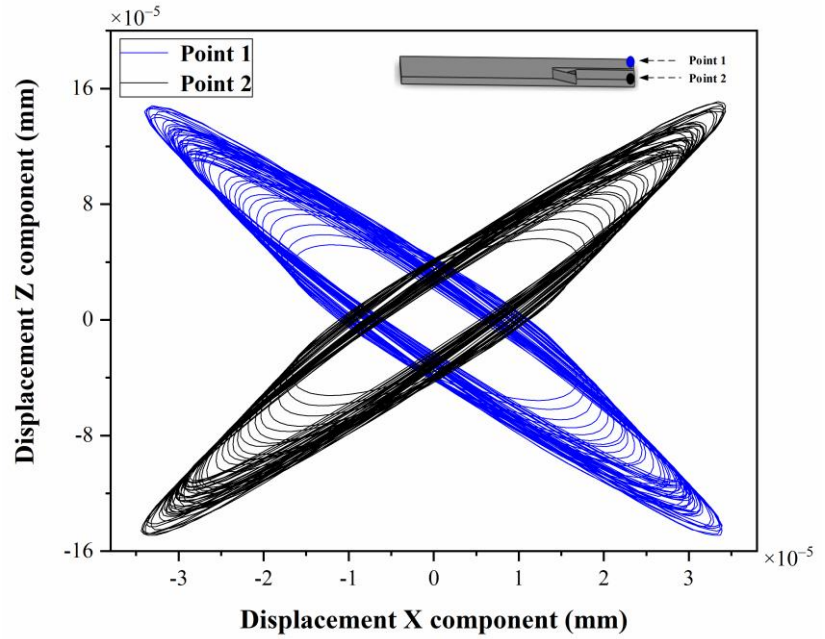


Figure 16. The vibration trajectories of tips.

4. Evaluation and Discussion

The designed micro-stirrer is designed to eventually be operated in narrow and fragile blood vessels. Therefore, testing the efficiency in such an environment is particularly important. However, the phenomenon is difficult to be measured in experiments, and it is necessary to make a closer analysis to evaluate its performance based on fluid-structure interaction. Therefore, a fluid-structure interaction analysis revolving around flow velocity and flow direction implemented in Comsol Multiphysics is introduced. Furthermore, a stirring test with a powerful driven force and a bigger stirrer size is conducted to verify the effect and accentuate the fluid phenomenon.

4.1. Fluid-Structure Interaction Simulation

The stirring and crushing functions of the micro-stirrer are the most important factors for accelerating clot dissolution. Previous research has confirmed that the scissor-type vibration can provide a more efficient crushing function and will not be the focus of this paper [26]. The turbulence induced by the micro-stirrer under scissor-type vibration mode is known to fully mix the blood clot with a thrombolytic agent, resulting in accelerated dissolution velocity. Therefore, a simulation with the micro-stirrer in a blood vessel is necessary.

The turbulence induced by the micro-stirrer is evaluated by a model with the end-effort and a blood vessel full of liquid. The physical properties of the liquid are set with a density of 1060 kg/m^3 and viscosity of 0.005 Ns/m^2, which are similar to real blood. To

reduce computation time, a power of 10 N with the resonance frequency replacing the PZT was added at the left cross-section of the stirrer as the input signal. The flow velocity and flow direction are then measured and recorded.

Figure 17 shows the simulation results of the fluid structure interaction model. As the scissor-type vibration is stable, the flow directions of liquid on the end-effort of two beam tips are opposite, which coincides with the vibration mode. The high flow velocity concentration on the tip of the end-effort is developed because of the high transverse amplitude at tips, and the flow velocity gradually decreases with the length increase far away from the stirrer tip. Moreover, the highest flow velocity with a value of 8.97×10^{-4} m/s occurs at the exit of the inner hole due to the pressure difference between the blood vessel and the inner hole. This also demonstrates that under the scissor-type vibration mode, the maximum flow velocity at the inner hole can provide auxiliary suction force for aspirating blood clot fragments.

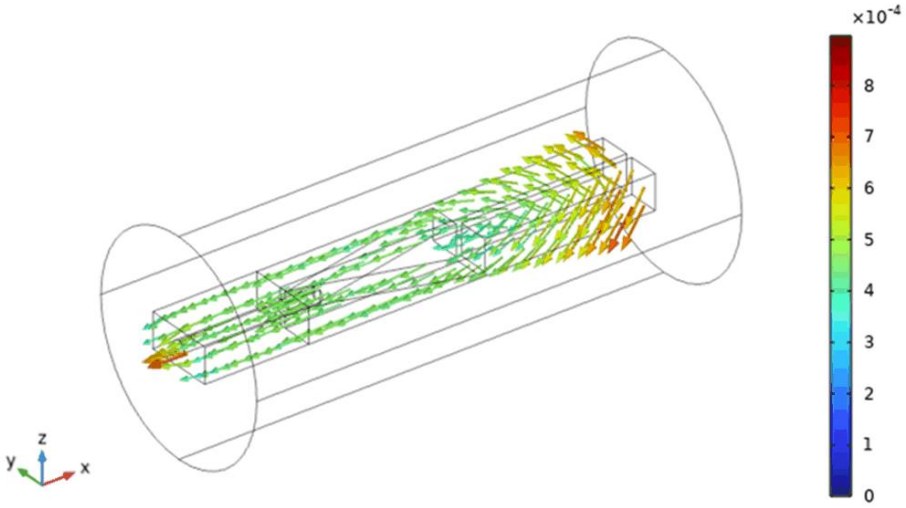


Figure 17. The flow velocity and flow direction of blood around the micro-stirrer end-effort.

As the flow velocity around the end-effort is induced by the motion of the stirrer, turbulence will be excited in the blood vessel, which will efficiently mix the clot fragments with a thrombolytic agent to accelerate dissolution. Further evaluation of this stir effect was conducted by simulating the turbulence phenomenon in the blood vessel. Figure 18 shows that the scissor-type vibration induces the flow of liquid, which further confirms the ability of the micro-stirrer to fully mix the clot fragments with the thrombolytic agent. Moreover, due to the opposite motion of the two tips at the end-effort, the blood flows reversely to the groove structure and forms an envelope shape. Therefore, it can be predicted that the fragments of the crushed clot will be stirred and flowed to the groove structure to follow the flow direction. The fragments are pushed to the aspirating entrance of the inner hole at the left end of the groove between two stirrer tips, which is better for aspirating fragments outside of the body.

4.2. Experiment Analysis

Further evaluation of the stirring performance was conducted by designing and manufacturing a prototype stirrer. The overall experiment setup is shown in Figure 19. The input signal was formed by a function generator (UTG 4082A) and then magnified by a power amplifier (HEAS-50). A laser vibrometer (LV-S01-KH), based on Doppler Effect, was utilized to test the resonance frequency of the micro-stirrer. For ease of experimental observations and cost-saving, a prototype with a bigger size was manufactured, comprising a back mass, a PZT, a front mass, a pre-stress structure and a beam with a scissor-type end-effort (Figure 20a). The PZT embedded in a hollow cylinder with a netted pre-stressed structure amplifies the driving vibration. The beam length, end-effort length, groove length, width and thickness of the stirrer beam were set as 20 mm, 7 mm, 2 mm, 3 mm and 0.5 mm,

respectively. The groove angle was 80°, and the material of the stirrer was stainless steel (SUS 304). To simulate blood and thrombus, a plastic container was filled with glycerol (thrombus) and a mixture of normal saline and red colorant (blood). The volume ratio of glycerol to the mixture was 1:1. In the experiment, the driving voltage was 50 V with the scissor-type vibration resonance frequency of 3558.9 Hz, and the end-effort tip was inserted into glycerol 1 mm under the surface of glycerol. When the scissor-type vibration is excited, the glycerol flows reversely to the groove structure and forms a similar envelope shape, which coincides with the above simulation result (Figure 20b). Therefore, the experimental stir performance and design efficiency coincide with the simulation results, further validating the design.

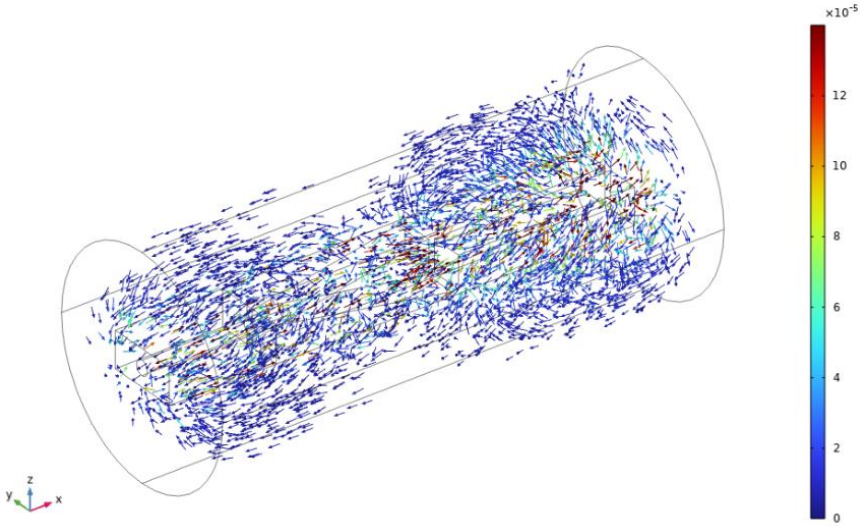


Figure 18. Full flow of fluid in a blood vessel.

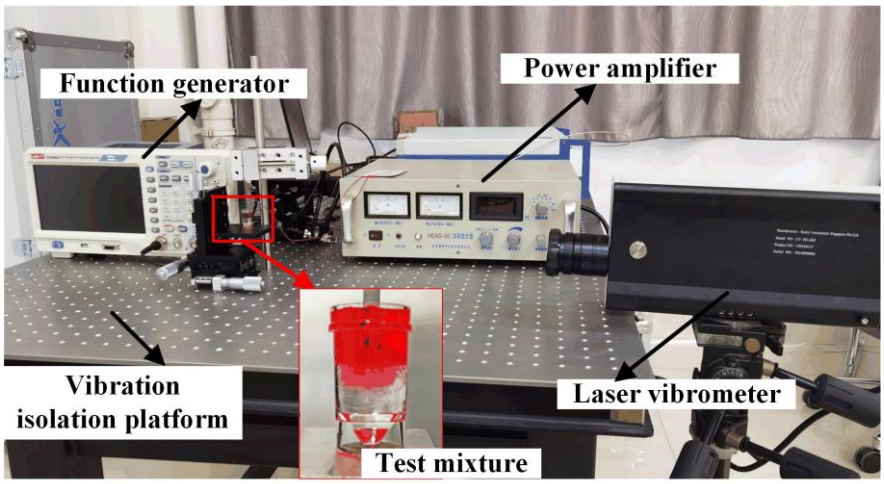


Figure 19. The experiment setup of stirring performance test.

4.3. Discussion of Advantages and Limitations

Over the past decades, many kinds of mechanical thrombectomy devices have been designed for acute ischemic stroke, such as Merci Retriever, Penumbra and Solitaire. These devices go beyond the time window of thrombolytics therapy and have a better therapeutic effect. The most recently designed devices, known as retrievable stents, have shown higher recanalization rates and better clinical outcomes than the older Merci retriever and Penumbra. However, most of these devices are used in relatively large cerebral vessels with diameters ranging from 2 mm to 5 mm. Moreover, many trials also show intima damage of blood vessels as the stent retriever threaded through the blood vessel. Compared with these

devices, the scissor-type micro-stirrer has many advantages. Firstly, according to the above study, the micro-stirrer can be designed and manufactured with a small size, which exhibits the potential for vascular recanalization in small blood vessels less than 2 mm. Secondly, due to the effective transverse vibration for dissolving thrombi concentrates on the end-effort of the stirrer, no intima damage of the blood vessel will be caused. Finally, since the mechanical vibration directly stirs the blood clot with a low dose of the thrombolytic agent, so that the clot could be dissolved more efficiently in a shorter time with a lower risk of hemorrhage than other devices. However, the micro-stirrer also has some potential limitations which should be studied deeply in the future. Firstly, considering the bended end-effort of the stirrer impacts the conversion efficiency of vibration mode, some curved blood vessels with small bending radius may not be suitable for this device. Secondly, the high-frequency vibration of the stirrer can induce effects including heating, cavitation and mechanical stress. It is unknown that whether these effects are helpful or harmful to the therapy. Therefore, many studies should be conducted as the next step toward further proving the therapeutic effect of micro-stirrer in stroke.

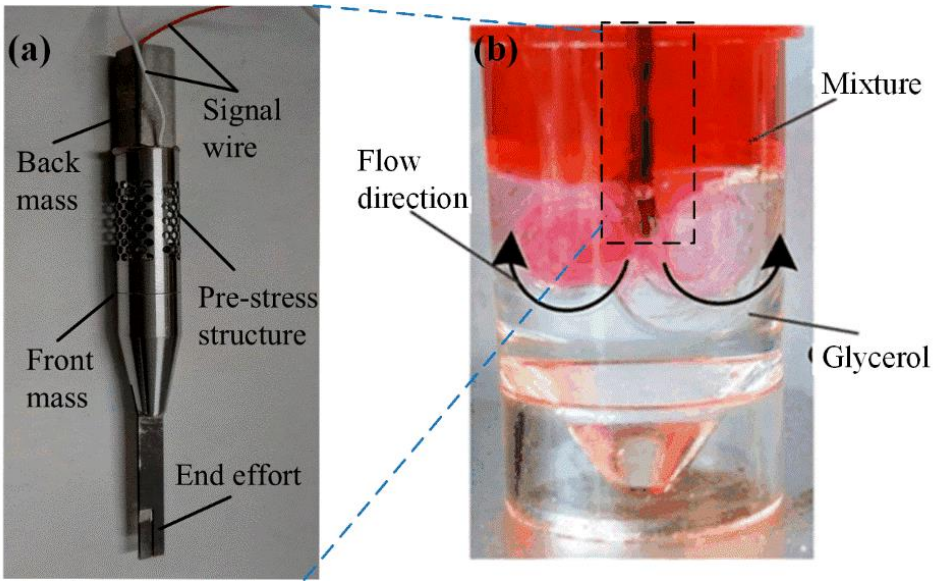


Figure 20. Stir performance test with (**a**) prototype of micro-stirrer and (**b**) visible flow turbulence.

5. Conclusions

A new design of micro-stirrer, which can supply stable and reliable scissor-type vibration for thrombus dissolution, is proposed in this paper. The theory of mode conversion is analyzed, and the important structure parameters involving incident angle, inertia mass, stiffness and inner hole are obtained. The optimal values of parameters are determined by a series of finite element simulations. For a length of end-effort of 10 mm, the optimal reflective angle of the groove, mass length, groove depth, and radius of the inner hole were determined to be 83°, 6 mm, 0.6 mm and 0.2 mm, respectively. The output transverse amplitude was further enhanced by extending the groove length verified. The analysis results also confirm that the aspirating inner hole partly decreases the conversion efficiency from longitudinal vibration to transverse vibration. Moreover, under the scissor-type vibration mode, the turbulence induced by vibration can fully mix clot fragments with a thrombolytic agent, and the fragments can be easily aspirated out of the body through the inner hole. In conclusion, the design method with optimal structural parameters to achieve the highest conversion efficiency and stir performance was obtained and verified with simulation and experimental design.

Author Contributions: Conceptualization, J.Y. and M.M.; methodology, J.Y. and B.R.; software, J.Y., B.R. and Y.J.; validation, L.W., Y.J., G.D. and J.Q.; formal analysis, J.Y. and Y.J.; investigation, J.Y., B.R. and L.W.; resources, J.Y.; data curation, B.R. and J.Q.; writing—original draft preparation, J.Y. and B.R.; writing—review and editing, J.Y.; visualization, L.W. and Y.J.; supervision, J.Y., J.Q. and M.M.; project administration, J.Y.; funding acquisition, J.Y. All authors have read and agreed to the published version of the manuscript.

Funding: This research was funded by the National Natural Science Foundation of China, Grant number: 51865021 and the Scientific and Technology Project of Yunnan Province, Grant number: 2019FD050.

Data Availability Statement: Data available on request from the authors.

Conflicts of Interest: The authors declare no conflict of interest.

References

1. Vos, T.; Lim, S.S.; Abbafati, C.; Abbas, K.M.; Abbasi, M.; Abbasifard, M.; Abbasi-Kangevari, M.; Abbastabar, H.; Abd-Allah, F.; Abdelalim, A.; et al. Global burden of 369 diseases and injuries in 204 countries and territories, 1990–2019: A systematic analysis for the Global Burden of Disease Study 2019. *Lancet* **2020**, *396*, 1204–1222. [CrossRef] [PubMed]
2. Lindsay, M.P.; Norrving, B.; Sacco, R.L.; Brainin, M.; Hacke, W.; Martins, S.; Pandian, J.; Feigin, V. World stroke organization (WSO): Global stroke fact sheet 2019. *Int. J. Stroke.* **2019**, *14*, 806–817. [CrossRef] [PubMed]
3. Mira, K.; Andreas, L. Global burden of stroke. *Semin. Neurol.* **2018**, *38*, 208–211.
4. Paul, S.; Candelario-Jalil, E. Emerging neuroprotective strategies for the treatment of ischemic stroke: An overview of clinical and preclinical studies. *Exp. Neurol.* **2021**, *335*, 113518. [CrossRef] [PubMed]
5. Zhao, Q.; Shan, W.; Liu, L.; Fu, X.; Liu, P.; Hu, Y. Predictors of functional outcome and hemorrhagic complications in acute ischemic stroke patients treated with intravenous thrombolysis—A retrospective analysis. *Int. J. Clin. Pharm. Ther.* **2017**, *55*, 893–900. [CrossRef]
6. Wang, R.; Zeng, J.; Wang, F.; Zhuang, X.; Chen, X.; Miao, J. Risk factors of hemorrhagic transformation after intravenous thrombolysis with rt-PA in acute cerebral infarction. *QJM Int. J. Med.* **2019**, *112*, 323–326. [CrossRef]
7. Gill, D.; Baheerathan, A.; Aravind, A.; Veltkamp, R.; Kar, A. Severe Hemorrhagic Transformation after Thrombolysis for Acute Ischemic Stroke Prevents Early Neurological Improvement. *J. Stroke. Cerebrovasc.* **2016**, *25*, 2232–2236. [CrossRef]
8. Park, T.H.; Lee, J.S.; Park, S.S.; Ko, Y.; Lee, S.J.; Lee, K.B.; Lee, J.; Kang, K.; Park, J.M.; Choi, J.C.; et al. Safety and Efficacy of Intravenous Recombinant Tissue Plasminogen Activator Administered in the 3 to 4.5 Hour Window in Korea. *J. Stroke. Cerebrovasc.* **2014**, *23*, 1805–1812. [CrossRef]
9. Clark, W.M.; Madden, K.P. Keep the Three Hour TPA Window: The Lost Study of Atlantis. *J. Stroke. Cerebrovasc.* **2009**, *18*, 170. [CrossRef]
10. Davis, S.M.; Donnan, G.A. 4.5 hours: The new time window for tissue plasminogen activator in stroke. *Stroke* **2009**, *40*, 2266–2267. [CrossRef]
11. Leys, D.; Deplanque, D. Thrombolysis beyond the three-hour time window. *Clin. Exp. Hypertens.* **2006**, *28*, 313–316. [CrossRef] [PubMed]
12. Katz, J.M.; Gobin, Y.P. Merci (R) retriever in acute stroke treatment. *Expert. Rev. Med. Devic.* **2006**, *3*, 273–280. [CrossRef] [PubMed]
13. Alshekhlee, A.; Pandya, D.J.; English, J.; Zaidat, O.O.; Mueller, N.; Gupta, R.; Nogueira, R.G. Merci mechanical thrombectomy retriever for acute ischemic stroke therapy: Literature review. *Neurology* **2012**, *79*, S126–S134. [CrossRef] [PubMed]
14. Son, S.; Choi, D.S.; Oh, M.K.; Hong, J.; Kim, S.K.; Kang, H.; Park, K.J.; Choi, N.C.; Kwon, O.Y.; Lim, B.H. Comparison of solitaire thrombectomy and penumbra suction thrombectomy in patients with acute ischemic stroke caused by basilar artery occlusion. *J. Neurointerv. Surg.* **2016**, *8*, 13–18. [CrossRef] [PubMed]
15. Nogueira, R.G.; Frei, D.; Kirmani, J.F.; Zaidat, O.; Lopes, D.; Turk, A.S.; Heck, D.; Mason, B.; Haussen, D.C.; Levy, E.I. Safety and efficacy of a 3 -Dimensional stent retriever with aspiration-based thrombectomy vs. aspiration -based thrombectomy alone in acute ischemic stroke intervention: A randomized clinical trial. *JAMA Neurolog.* **2018**, *75*, 304–311. [CrossRef]
16. Pereira, V.M.; Yilmaz, H.; Pellaton, A.; Slater, L.A.; Krings, T.; Lovblad, K.O. Current Status of Mechanical Thrombectomy for Acute Stroke Treatment. *J. Neuroradiol.* **2015**, *42*, 12–20. [CrossRef]
17. Arai, D.; Ishii, A.; Chihara, H.; Ikeda, H.; Miyamoto, S. Histological Examination of Vascular Damage Caused by Stent Retriever Thrombectomy Devices. *J. Neurointerv. Surg.* **2016**, *8*, 992–995. [CrossRef]
18. Mechanical Thrombolysis in Acute Stroke. Available online: http://emedicine.medscape.com/article/1163240-overview#a1 (accessed on 8 May 2017).
19. Jiang, Z.W.; Liu, Z.H.; Kato, S.; Suzuki, M. Fundamental Study on a Novel Method for Dissolution of Cerebral Thrombus by Micro Piezo-stirrer. In Proceedings of the JSME-IIP/ASME-ISPS Joint Conference on Micromechatronics for Information and Precision Equipment, Yokohama, Japan, 16–18 June 2003.
20. Jiang, Z.W.; Morita, M.; Watanabe, T.; Kato, S.; Suzuki, M. Study on In-vivo measurement of solubility for cerebral thrombus dissolution. *Int. J. Appl. Electrom.* **2006**, *24*, 225–234. [CrossRef]

21. Yang, J.J.; Morita, M.; Jiang, Z.W. Design of a novel scissoring micro-stirrer for blood clot dissolution. *Sens. Actuator. A Phys.* **2016**, *248*, 130–137.
22. Morita, M.; Yang, J.J.; Fujioka, Y.; Jiang, Z.W. A novel mechanical thrombectomy device based on complex longitudinal-torsional vibration. *J. Adv. Mech. Des. Syst.* **2018**, *12*, JAMDSM0086. [CrossRef]
23. Ajoudanian, M.; Jiang, Z.W.; Morita, M. Study on a new type micro-stirrer excited by longitudinal elastic wave for thrombus dissolution. *Int. J. Appl. Electrom.* **2011**, *37*, 67–77. [CrossRef]
24. Ajoudanian, M.; Jiang, Z.W.; Morita, M. Design of a novel type micro-stirrer excited by longitudinal elastic wave for thrombus dissolution. *J. Biomech. Sci. Eng.* **2011**, *6*, 262–269.
25. Jen, C.; Kobayashi, M. *Ultrasonic and Advanced Methods for Nondestructive Testing and Material Characterization*, 1st ed.; Chen, C.H., Ed.; World Scientific Publisher: Singapore, 2007; Volume 1, pp. 33–40.
26. Yang, J.J.; Xu, T.J. A novel phacoemulsification needle with scissor-like motion end effector for reducing heat generation at cornea incision. *Sens. Actuator. A Phys.* **2019**, *288*, 92–100. [CrossRef]

Disclaimer/Publisher's Note: The statements, opinions and data contained in all publications are solely those of the individual author(s) and contributor(s) and not of MDPI and/or the editor(s). MDPI and/or the editor(s) disclaim responsibility for any injury to people or property resulting from any ideas, methods, instructions or products referred to in the content.